Research Square

Preprints are preliminary reports that have not undergone peer review.
They should not be considered conclusive, used to inform clinical practice,
or referenced by the media as validated information.

Coupling between Free Tropospheric Warming and Elevated Surface Warming

Pietro Martuzzi

pietro.martuzzi@mpimet.mpg.de

Max Planck Institute for Meteorology: Max-Planck-Institut fur Meteorologie

Marco A. Giorgetta

Max Planck Institute for Meteorology: Max-Planck-Institut fur Meteorologie

Research Article

Keywords: Elevation Dependent Warming (EDW), High resolution modeling, Free tropospheric warming, P4K Amip Experiment, Surface-troposphere coupling

Posted Date: February 24th, 2026

DOI: https://doi.org/10.21203/rs.3.rs-8788774/v1

License: This work is licensed under a Creative Commons Attribution 4.0 International License.
Read Full License

Coupling between Free Tropospheric Warming and Elevated Surface Warming

Pietro Martuzzi[1] and Marco A. Giorgetta[1]

[1]Max Planck Institute for Meteorology, Bundesstraße 53, 20146, Hamburg, Germany.

Contributing authors: pietro.martuzzi@mpimet.mpg.de;

Abstract

Elevation-dependent warming (EDW) has been reported in observations and climate models, yet its magnitude and controlling mechanisms remain uncertain, particularly due to the complexity of mountain regions. However both theoretical studies and climate simulations indicate a reduction in lapse rates and enhanced tropospheric warming under climate change. In this study, we examine EDW in atmosphere-only experiments as the comparison between a historical control simulation and a climate state driven by uniform 4K warming in the prescribed sea surface temperatures. These simulations were performed with the ICON model in its Sapphire configuration at ∼10 km horizontal grid spacing. This setup offers an improved representation of high-elevation terrain compared to common climate change simulations, key to adequate analysis of EDW, together with a strong free-tropospheric warming, important for understanding its role in shaping EDW. The simulation exhibits a robust, statistically significant increase in surface warming with elevation, ranging from ∼4.9 K below 500 m to almost 7 K above 5500 m, corresponding to a global EDW slope of 0.317 K km^{-1}. Regional contrasts are most pronounced at low elevations, while at intermediate and high elevations the surface warming profiles converge toward the tropospheric warming. Seasonal variations suggest an influence from snow-related processes, yet the majority of the seasonal variability in surface warming can be explained by seasonal variations in tropospheric warming. A direct comparison of binned surface and tropospheric temperature changes at corresponding heights reveals a tight coupling, with small deviations possibly resulting from radiative processes near the surface. These results indicate that, under strong free-tropospheric warming, EDW can be approximated to first order by the vertical structure of tropospheric warming, with surface energy-balance processes largely providing secondary modulation. The sensitivity of this coupling to different forcing magnitudes and climate states warrants further investigation.

Keywords: Elevation Dependent Warming (EDW), High resolution modeling, Free tropospheric warming, P4K Amip Experiment, Surface-troposphere coupling

1 Introduction

The surface warming response resulting from changes in the global climate is not spatially homogeneous (IPCC 2023), and certain land regions such as the Arctic are more sensitive than others (Pepin et al. 2022). There is also growing evidence that warming rates vary with elevation, more specifically that higher elevations and mountain environments often experience enhanced warming, a phenomenon commonly referred to as "Elevation Dependent Warming" (EDW) (Pepin et al. 2015). This poses threats to ecosystems, the cryosphere, and most importantly to the hydrological security of millions of people (IPCC 2022; Pepin et al. 2022; La Sorte and Jetz 2010).
On one hand, the similarities in underlying climates between the Arctic and high-elevation regions could hint at this phenomenon. On the other hand, the heterogeneity and complexity of climate patterns in mountain environments create many uncertainties and challenges in understanding and quantifying EDW (Pepin et al. 2022). Furthermore, due to the remoteness of mountain areas, dense observational networks with long-term measurements are generally unavailable, and the available data may not be representative of broader trends due to the effects of microclimates and small-scale spatial variability common in mountain environments (IPCC 2022; Whiteman 2000). This is both an issue for observational studies and for models, which require observations for their validation.

Despite these challenges, EDW has been detected in several observational studies (Pepin et al. 2015; Wang et al. 2014, 2016; Qixiang et al. 2018; Ohmura 2012; Liu et al. 2009; Liu and Chen 2000; Rangwala et al. 2009). However, different methodologies and contradicting results have made observational studies not (yet) sufficient to provide certainty that EDW is a robust response to climate change, and they still appear far from allowing us to gain a quantitative understanding of it and its driving mechanisms. Different methodologies result from the varying goals of the studies, as well as the regions, time periods, and temperature variables (T, $T_{\min}$, or $T_{\max}$) analyzed. Some studies attempt to determine whether (and how much) warming is amplified along an elevation gradient (e.g. Qixiang et al. 2018; Ohmura 2012), while others simply compare the mean warming rate across a high-altitude region to the corresponding latitudinal or global mean (e.g. Ceppi et al. 2012). Moreover, contradicting results exist, reporting maximum warming at an intermediate elevation, often near the 0,°C isotherm (e.g. Pepin and Lundquist 2008), or reporting higher warming rates at low elevations (Rottler et al. 2019; Tudoroiu et al. 2016).

Models provide tools to study EDW and its driving mechanisms, mitigating some of the key shortcomings and challenges inherent to observations in topographically complex environments, though they still rely on measurements for their validation. Problems related to modeling studies are usually linked to resolution with many

climate models still struggling to resolve complex topography and its associated processes (e.g., orographic precipitation, snow accumulation) due to their limited horizontal resolution (Palazzi et al. 2017; IPCC 2022). While RCMs can often be run at higher resolutions allowing them to explicitly resolve more of the processes inherent to complex mountain environments, this presents a particular challenge for GCM studies. The review paper by Pepin et al. (2015) claims that the climate response within complex mountain topography can only be adequately captured using models with a spatial resolution of 5 km or less, which generally implement non-hydrostatic equations for the atmosphere. This suggests that most (if not all) GCM (and many Regional Climate Model (RCM)) studies with much coarser resolutions cannot adequately capture EDW. The role of model spatial resolution itself has also been the focus of several studies, most of which report that the structure and magnitude of the simulated EDW signal vary depending on resolution (Palazzi et al. 2019; Minder et al. 2018; Yan et al. 2016). In fact, Yan et al. (2016) note that at their lowest resolution (T31, $\sim$ 350 km) the climate model is unable to capture EDW over the Tibetan Plateau, and attribute this to poor representation of topography and its effect on surface-radiation–related processes. Minder et al. (2018) used a RCM with much higher resolutions (between $\sim$ 36 km and $\sim$ 4 km), comparable to the that used in this paper and also attributed differences between resolutions to topographic representation. For instance, they argue that at lower resolution, where high mountain peaks are not represented, the accumulation of deep mountaintop snowpack is limited due to reduced orographic precipitation and increased snowmelt from warmer temperatures. Similarly, in the paper by Palazzi et al. (2019), the snow–albedo feedback in the Alps during summer was only detectable at the highest resolution ($\sim$ 16 km), owing to its improved representation of high elevations.

In spite of the role of resolution, and likely as a result of the larger amount of available data and the ability to simulate both past and future climates, modeling studies tend to be much more in agreement about EDW being a robust response to climate change across various models, simulations and methodologies (Pepin et al. 2015; Giorgi et al. 1997; Kotlarski et al. 2012; Rupp et al. 2017; Minder et al. 2018; Yan et al. 2016; Rangwala et al. 2010; Liu et al. 2009; Rangwala et al. 2013; Palazzi et al. 2019; Rangwala et al. 2016; Byrne et al. 2024). Instead, they present inconsistencies in their attribution of the warming differentials to various mechanisms and their interactions. As discussed in Kotlarski et al. (2012), the near-surface temperature altitude gradient is constrained by the free tropospheric gradient and modulated by surface local effects on various time and spatial scales. As a result, the local temperature changes in mountain environments are suggested to result from a combination of changes to the large-scale environmental lapse rate and more small-scale effects related to surface energy balance changes (Kotlarski et al. 2012). In this study we propose the following equation to analyze these effects:

$$\Delta T_s(\phi, \lambda, h) = \alpha \Delta T_a(\phi, h) + \beta(\phi, \lambda, h) \tag{1}$$

where $\Delta T_s(\phi, \lambda, h)$ is the surface warming at a given latitude ϕ, longitude λ, and height above sea level h. $\Delta T_a(\phi, \lambda)$ is the large-scale tropospheric warming at the

corresponding height and latitude, averaged over a broader longitude range where its variability is expected to be low. α represents a coupling coefficient between tropospheric and surface warming, and β represents all terms affecting the surface energy balance at a given location and their effect on temperature. This term is extremely complex and encompasses radiative effects from feedbacks (e.g., snow-albedo, humidity, or cloud feedbacks) as well as the partitioning of additional absorbed surface energy into sensible and latent heat fluxes. This β term, more specifically through the snow–albedo feedback, is often reported as the most important driving mechanism of EDW in both global coarser-resolution models (Yan et al. 2016; Liu et al. 2009; Palazzi et al. 2017; Byrne et al. 2024; Rangwala et al. 2010) and higher-resolution regional simulations (Giorgi et al. 1997; Kotlarski et al. 2012; Rupp et al. 2017; Minder et al. 2018). This has been demonstrated through both statistical analyses (e.g. Palazzi et al. 2017; Rangwala et al. 2010) and a radiative kernel analysis (Byrne et al. 2024), largely due to the strong influence of snow–albedo feedback near the 0,°C isotherm on the surface radiation balance.

While the importance of the snow–albedo feedback is consistently addressed in the literature, the roles of other driving mechanisms remain more uncertain. Cloud (Duan and Wu 2006; Yan et al. 2016; Byrne et al. 2024; Liu et al. 2009) and humidity (Palazzi et al. 2017; Rangwala et al. 2010, 2009; Byrne et al. 2024) changes are often mentioned in relation to elevation-dependent warming, though studies frequently offer very different interpretations of their roles in driving or opposing EDW. Some studies also report large-scale changes to lapse rates (tropospheric warming ΔT_a) as a driver of EDW (Kotlarski et al. 2012; Rupp et al. 2017; Minder et al. 2018), though this remains largely unaddressed and misunderstood. Many climate simulations and theoretical studies indicate a reduction in lapse rates under climate change and an enhanced tropospheric warming compared with the surface (Frierson 2006; Colman and Soden 2021). In tropical regions, this occurs due to the increased latent heat release associated with the condensation of moister air parcels as atmospheric moisture content increases (Colman and Soden 2021). Because convection approximately constrains the tropical environmental lapse rate to the moist adiabat, this can also be understood through the temperature dependence of the moist adiabatic lapse rate, whereby an increase in temperature leads to a decrease in the lapse rate (Held and Soden 2006; Colman and Soden 2021). In the midlatitudes, the observed and simulated decrease in lapse rate (Frierson 2006) can be better explained by the presence of convective cores associated with baroclinic eddies, which contribute to enhanced warming in the upper troposphere (Colman and Soden 2021). Although these changes are mainly analyzed in the context of the induced negative lapse-rate feedback, this study will focus on whether this enhanced tropospheric warming is projected onto elevated surfaces that extend into the free troposphere—the term α in Equation 1. This mechanism is often found to explain only a secondary part of the warming signal, with surface warming being more pronounced and more spatially variable than tropospheric warming at equal heights (Kotlarski et al. 2012; Rupp et al. 2017; Minder et al. 2018). However, in a regional study of the tropical Andes in Ecuador, Chimborazo et al. (2022) found that tropospheric warming does project

onto the surface, enhancing EDW in both RCP4.5 and RCP8.5 scenarios.

In this study, we use an idealized climate simulation consisting of a uniform 4K warming in the prescribed sea surface temperature (P4K) compared to a control simulation (CNTL), which use the global atmosphere model ICON at $\sim$ 10 km horizontal grid spacing. This represents an unprecedented dataset in the study of EDW, as such resolution is hardly ever reached by GCMs and is still uncommon in RCM studies. Despite not reaching the 5 km resolution suggested by Pepin et al. (2015), this simulation should provide a more adequate representation of the warming response in complex mountain environments compared to those presented in many GCM and RCM studies. Merlis et al. (2024) provides an analysis of the tropospheric warming response in a P4K simulation, highlighting a strong tropospheric warming and decreasing lapse rates comparable to those simulated in CMIP6. This therefore provides a unique opportunity to analyze the warming response and its dependence on elevation, as well as the coupling between tropospheric warming and surface warming, leveraging both the high spatial resolution and the strong tropospheric warming in the simulation. The latter enhances the signal-to-noise ratio of the vertical temperature response and thus allows a clearer assessment of the coupling between free-tropospheric and surface warming.

The paper is organized as follows, section 2 presents the simulation data (2.1), the study areas (2.2) and the quantification methods (2.3) of this study. The results are presented in section 3 where first a global, annual quantification of the simulated EDW is shown. In subsection 3.1 the regional and seasonal variations of EDW and their implications for the drivers are analyzed and discussed while subsection 3.2 addresses the coupling between the tropospheric warming and surface warming. Section 4 provides a conclusion, summarizing the paper and discussing its results and outlook.

2 Methods

2.1 Simulation data

The outputs of a historical and a perturbed climate simulation are analyzed. Both simulations are performed using the ICON model (Giorgetta et al. 2018) in an atmosphere-only (AMIP) configuration. They are conducted on the ICON R02B08 grid, which has a horizontal resolution of $\sim$ 10 km (Giorgetta et al. 2018, Table 1). The simulations use the ICON-Sapphire configuration (Hohenegger et al. 2023), which aims to represent the Earth system and its interactions at 10 km scale or finer. This configuration explicitly simulates convective processes while retaining parameterization schemes for radiation, microphysics and turbulence. As a result of the AMIP setup, the control simulation (referred to as CNTL) is a historical run from 1979 to 1997 using observed transient sea surface temperatures (SST), sea ice concentrations (SIC), and greenhouse gas (GHG) levels from Taylor et al. (2000). Consequently, it includes some degree of anthropogenic forcing. The perturbed simulation is achieved using the same setup, but with a homogeneous +4 K SST increase, giving it the name P4K. This produces a strong warming response intended to overwhelm internal variability and highlight the system's response. Unlike a traditional forcing experiment, the warming arises from boundary-condition changes that induce a radiative imbalance in the P4K simulation. Unlike the CNTL simulation, the P4K simulation only runs through the end of 1993. The simulation outputs are provided on a HEALPix grid with zoom level 8, on 26 model levels and with a daily output frequency, to save storage memory.

Due to the use of uncoupled sea ice concentrations, high-latitude regions where climate is strongly influenced by sea ice, will be excluded from the analysis to preserve the validity of the study. Therefore, in the results section, "global" analysis refers to latitudes below 50°.
For comparability, both CNTL and P4K will be limited to the 14-year period from 1980 to 1993. The year 1979 is excluded to allow for model spin-up, as the P4K simulation is assumed to be partly in a transient state during this time. During the remaining 14 years, the climate is assumed to be approximately in thermal equilibrium, allowing for comparisons between the two different climate states.

2.2 Study areas

In this study, the global analysis of EDW is complemented by the exploration of specific mountain regions of the world in order to gain a better understanding of its regional characteristics and differences. These regions are the European Alps (Alps), high-mountain Asia including the Himalayas and Tibetan Plateau (Tibet), the North American Rocky Mountains (Rockies), and the Andes. These regions are selected to allow for comparisons across different hemispheres as well as between areas at similar latitudes. The selected extent and orography of each of these regions are shown in Figure 1.

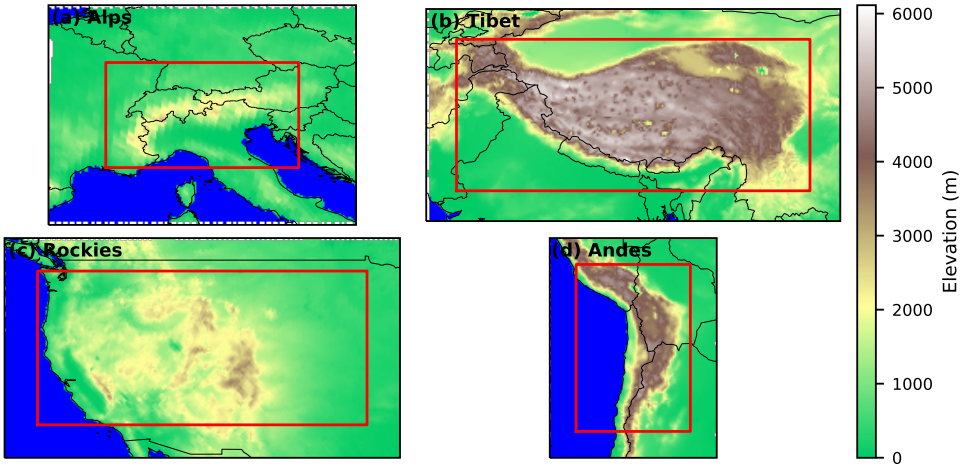


Fig. 1 Model topography for the four mountainous regions considered in this study. The red boxes indicate the latitude–longitude masks applied in the analysis: (a) Alps (43.5–49°N, 4.9–15°E), (b) Tibet (25–40°N, 70–105°E), (c) Rockies (34–48°N, 235–265°E), (d) Andes (13–32°S, 284–297°E)

2.3 Quantifying the warming signal

The first step in any EDW study is to detect a warming signal, either as a trend in transient experiments or as a difference between two climate states. In this study, the warming signal is computed as the difference between the climatological 2-m temperatures of the P4K and CNTL simulations:

$$\Delta T_s = \bar{T}_{P4K} - \bar{T}_{CNTL} \tag{2}$$

where the bar represents a time-averaged value. The second step is then to assess whether this warming exhibits a dependence on elevation. Various approaches have been used to do so: early studies often compared the warming rates of high-elevation regions to global or latitudinal means, while more recent and widely used methods involve plotting warming trends or temperature changes against elevation. In this study, the altitudinal dependence of the warming is computed as follows: the warming ΔT_s of individual grid points is grouped into 500-m elevation bins based on their model orography. For each bin, the mean warming is plotted against the bin elevation midpoint. Finally, a linear regression is applied, with the slope representing a metric that quantifies EDW (the same method used in Chimborazo et al. (2022)).

The simulation output of 3-dimensional atmospheric fields is provided on hybrid model levels. As such, vertical levels do not correspond to fixed geometric heights, but their local heights depend on the surface elevations. The same vertical binning used for surface warming based on cell elevation is also applied to the 3-dimensional temperature field based on geometric height for the comparison of the atmospheric warming profile to the EDW.

3 Results

As described in subsection 2.3, EDW is analyzed by plotting bin-averaged near-surface warming rates against elevation and quantifying the slope by a linear regression. The annual, global plot of warming rates against elevation is shown in Figure 2. The black dots in the figure represent the mean warming in each bin plotted against the bin-midpoint elevation. The dashed blue line represents the linear regression of these points, where the linear approximation appears to be a good fit to the binned data. This figure shows an almost linear and statistically significant ($p < 0.001$) trend of warming enhancement with surface elevation. This finding is consistent with several studies (e.g. Palazzi et al. 2019; Byrne et al. 2024), although it contradicts studies that indicate enhanced warming at intermediate elevations (e.g. Pepin and Lundquist 2008). The near-surface warming is approximately $\sim$ 4.9 K at elevations below 500 m and nearly 7 K above 5500 m, with a regressed slope of 0.317 K/km indicating substantial amplification of warming with elevation. While this appears broadly consistent with previous estimates (e.g. Wang et al. 2016), differences in data sources and methodologies make direct comparisons less meaningful. For example, Wang et al. (2016) reported a global slope of 0.23 K/km between 1961–2010, but using observations from weather stations.

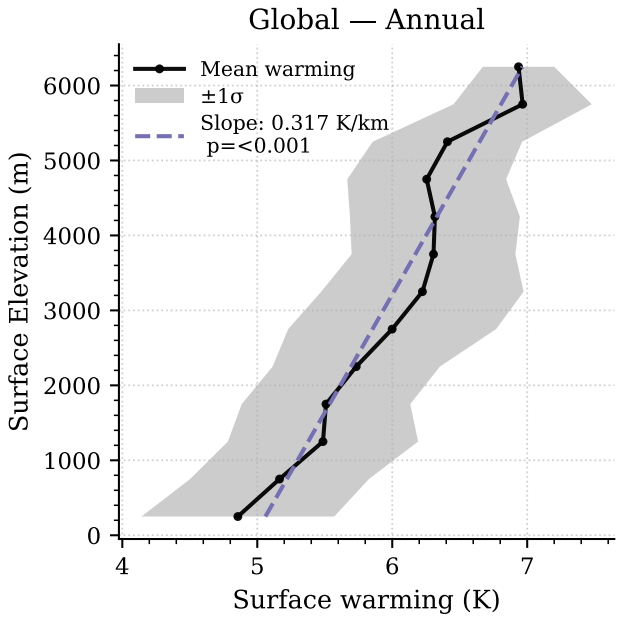


Fig. 2 2m temperature differences ΔT_s (from eq. 2 binned by model cell elevation, plotted as bin mean against bin midpoint elevation (black dots). The shaded area represents the standard deviation within each bin. The blue line is a linear regression of the black dots and corresponds to the quantification of EDW

3.1 Regional & Seasonal Analysis

In order to develop a better understanding of EDW and its drivers, more specifically its coupling to tropospheric warming, a regional and seasonal analysis is performed. Figure 3a shows the annual warming rates plotted against elevation for the regions described in subsection 2.2. Although the regressed line is not explicitly shown in this plot as in Figure 2, the corresponding slopes for each region are presented in the legend. The simulated slope of 0.29 K/km for Tibet is consistent with that found in Yan et al. (2016) (0.27 K/km) in a 4xCO2 simulation, though at much coarser resolution. Moreover, the slope of 0.542 K/km for the Alpine region closely matches the ∼0.5 K/km found in Giorgi et al. (1997) using a 2xCO2 RCM simulation, again at coarser resolution.

The differences in EDW between regions, as quantified by the regressed slopes, appear quite large, with the strongest signal present in the Rockies (0.82 K/km) and the weakest in Tibet (0.29 K/km), despite both being located at similar latitudes. However, Figure 3a indicates that these regional differences are primarily driven by absolute differences in the lowest elevation bins, while at intermediate elevations regional contrasts are far less pronounced. At the highest elevations, present only for the Andes and Tibet, differences appear very large, though this is likely a consequence of little statistics over fewer data points. Both of these regions only have 3 land cells in the highest elevation bin (see Table A1). At intermediate elevations, the close alignment of regional warming profiles points to the influence of a common driver with relatively small spatial variability. As such, it hints at the role of the free troposphere in governing near-surface temperature changes. Tropospheric warming is spatially more uniform, particularly in the tropics where temperature gradients are weak, entrainment into the boundary layer effectively transfers this uniformity downward, constraining surface warming to values similar to those aloft (further discussed in subsection 3.2). Figure 3b shows the seasonal variations of warming against elevation for the northern extratropics (30°–50°), to ensure a clear seasonal cycle in temperatures. This suggests that the strongest EDW occurs during autumn (SON), followed by spring, summer, and winter. However, most studies find the strongest EDW in the cold season or during the transition seasons, especially spring, and attribute this to the influence of snow and the snow–albedo feedback (e.g. Palazzi et al. 2019; Yan et al. 2016). In this case however, the linear regression approach to quantifying EDW appears to omit important details of the warming signal. For example, the regression slopes in SON and JJA are strongly influenced by the highest elevation bins, which may not be representative due to limited sampling from specific mountainous areas. Furthermore, below ∼3500 m the slope is largest in DJF, and even up to ∼5750 m MAM exhibits a larger EDW than SON. The pattern observed in DJF (and to some extent in MAM) is possibly related to snow effects: the pronounced decrease in slope above ∼3500 m could reflect temperatures remaining too low at such elevations for significant snow cover reduction between the simulations, reducing the strength of the snow-albedo feedback.

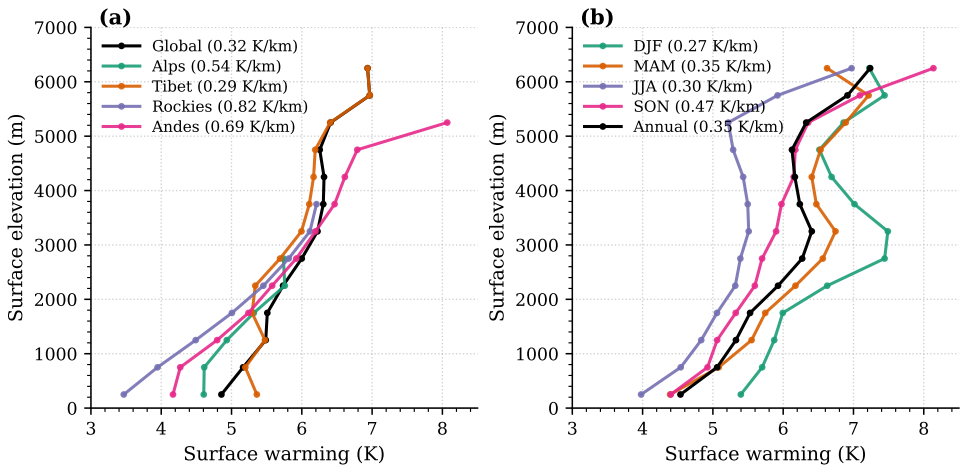


Fig. 3 (a) Regional comparison of annual EDW using the method from Figure 2. The colored lines represent the binned averaged ΔT_s against cell elevation. The linear regressions are not displayed but the corresponding slopes are presented in the legend. (b) Same as (a) but the seasonal comparison of ΔT_s against elevation. The data here only represents the northern extratropics (30°–50°N) where seasons are well defined by varying temperatures

3.2 Coupling between free tropospheric and surface warming

The regional analysis of EDW hinted at the role of free-tropospheric warming in driving near-surface warming, while the seasonal analysis appeared consistent with previous studies linking warming variability to snow effects. To better understand the role of the free troposphere, Figure 4a adds the globally averaged tropospheric warming profile over land to Figure 3a. The figure appears to corroborate the hypothesis of a strong influence of tropospheric warming on near-surface warming, showing the convergence of ΔT_s toward ΔT_a above ∼2000 m and below ∼5000 m, where deviations may be explained by averaging over far fewer data points. Figure 4b plots both the extratropical (30°–50°N) surface warming (ΔT_s) against elevation, as in Figure 3b, and also the tropospheric warming (ΔT_a) for each season averaged over this region. Figure 4b suggests that seasonal differences in tropospheric warming are projected onto near-surface warming, constraining it, as also found by Chimborazo et al. (2022). The noticeable deviations from the corresponding tropospheric warming profiles are attributable to varying coupling strengths and energy balance processes across seasons. The previous discussion about the role of snow cover changes in shaping near-surface warming remains applicable and can be understood as causing departures from the tropospheric warming profile. In JJA and SON, for example, deviations from the tropospheric warming profiles are small—except at the highest elevations—indicating strong coupling ($\alpha \approx 1$) and a weak contribution of other processes ($\beta \approx 0$), consistent with a limited influence of snow cover changes during those seasons. Nevertheless, accurately quantifying the relative roles of the many mechanisms operating at different spatial and temporal scales remains very challenging.

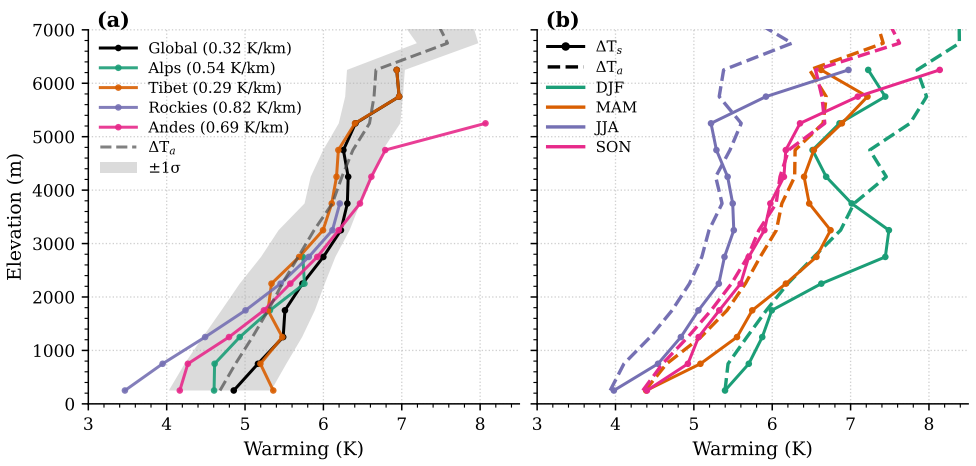


Fig. 4 As in Figure 3 with (a) globally and annually averaged profile of atmospheric temperature changes (ΔT_a) over land, and standard deviation. As described in subsection 2.3, the tropospheric warming profile is computed similarly to surface warming using 500m elevation bins based on each point's geometric height. In (b), the tropospheric warming profiles for each season are added as dashed lines. These are computed as the bin averages in the region defined by the latitude constraints ($30° - 50°$N)

To further analyze this coupling, the binned surface warming and binned tropospheric warming values are plotted against each other in Figure 5. Regional tropospheric warming is computed using the regional masks defined in subsection 2.2, but with an expanded longitudinal extent ($\pm 30°$) to better capture large-scale temperature changes. As latitude bands we use: tropics (15°S–15°N), southern and northern subtropics (15°–30°S/N), and extratropics (30°–50°S/N) are also included in the analysis. Having ΔT_s and ΔT_a binned in identical elevation bins, allows for regional and seasonal comparison of these values to understand the role of ΔT_a in shaping the variability in ΔT_s. As such, the bin-means at corresponding elevations are plotted against each other. With the addition of seasonal variations and regional subdomains, Equation 1 can be generalized as:

$$\Delta T_s(\phi_1, \phi_2, \lambda_1, \lambda_2, h, t) = \alpha(\phi_1, \phi_2, \lambda_1, \lambda_2, h, t)\, \Delta T_a(\phi_1, \phi_2, \lambda_1 - 30°, \lambda_2 + 30°, h, t) + \beta(\phi_1, \phi_2, \lambda_1, \lambda_2, h, t) \tag{3}$$

where t represents the season, the subscripts 1 and 2 represent the maximum and minimum (latitude and longitude) of the chosen region, and where α and β are allowed to vary across all spatial dimensions and timescales. For example, α depends on boundary layer entrainment, which itself depends on seasonality, cloudiness, diurnal cycle, inversions, topography, and surface characteristics. β is related to surface energy balance processes, which can exhibit strong spatial and temporal variability, especially in complex mountain terrain.

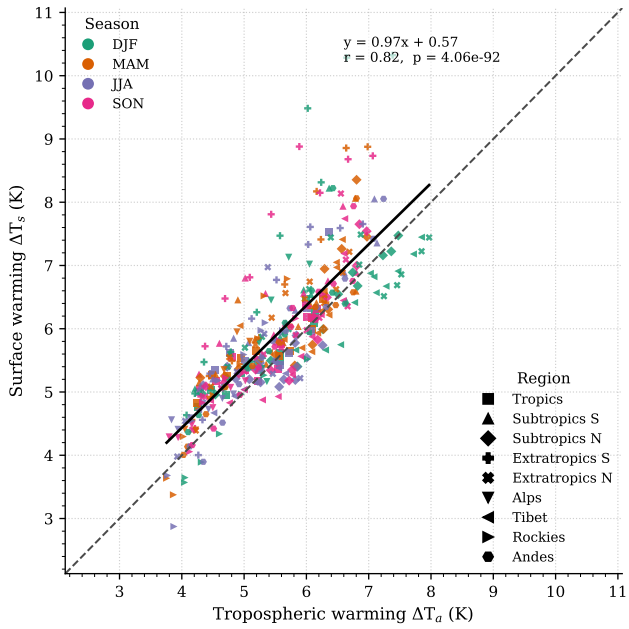


Fig. 5 Scatter plot of surface (2m) warming vs tropospheric warming at various heights, for all the seasons and various regions. Regions also include latitude bands on top of the regions described in subsection 2.2. Height is not show in the plot, but the two warming values are plotted as the means of identical height bins, e.g. for the 2000-2500m a.s.l. bin, the mean surface warming and mean tropospheric warming are plotted. The same is done for all bins

Figure 5 shows this scatter plot fitted with a linear regression, which averages α and β from Equation 3 over all degrees of freedom. The plot indicates a very strong coupling between tropospheric warming and surface warming, as many points fall near the diagonal 1-to-1 line (dashed line), or slightly above it, suggesting on average $\beta > 0$ and thus a positive contribution of surface-energy-balance processes (e.g., snow–albedo feedback) to temperature changes. Deviations from the 1-to-1 line are attributable both to physical processes and to averaging over a small number of grid points in certain bins, which may reflect highly localized behavior rather than regional or seasonal trends. Many of the points showing strong positive deviations from the 1-to-1 line are found in the southern extratropics (30°–50°S), where ΔT_s is systematically higher than ΔT_a and the difference increases with warming (and hence with elevation). Despite this region containing fewer data points than others, as visible in Table A1, and being mostly representative of the southern Andes, understanding this specific regional behavior lies beyond the scope of this study.

Nonetheless, the results suggest that, globally and to first order, tropospheric warming is a good approximation for surface warming at the corresponding elevation: $\Delta T_s(h) \approx \Delta T_a(h)$ as it explains much of the seasonal and regional variability in surface warming. The linear regression yields $\alpha = 0.97$ and $\beta = 0.57$ K. However, as previously noted, this approach averages α and β over all regions, seasons, and elevations, even though they depend on these parameters. Despite being outside the scope of this paper, it

would be more meaningful to explore how these terms vary with height, seasonally or regionally.

4 Conclusion

In this study, the ICON model was used in its AMIP, Sapphire configuration at ~ 10 km resolution to investigate the amplification of warming along a surface elevation gradient, and its relation to tropospheric warming at corresponding elevations. The high resolution is understood to allow for a significantly better depiction of the complex terrain in mountain areas and its associated processes compared to the majority of present studies done with both global and regional climate models, though its role is not explored in this paper. There exist many studies highlighting the presence of EDW, both using observational and modeling data, each with their respective challenges. Building on these studies, EDW is generally expected as a response to climate change, although its magnitude and underlying mechanisms remain poorly constrained. Many studies attribute the enhancement of warming with elevation to snow-cover changes and the snow albedo feedback, with few others mentioning large-scale lapse rate changes, cloud effects and the water vapor feedback. This study aimed to better understand EDW and how large-scale tropospheric warming could affect this phenomenon in an idealized P4K simulation. Such simulation is used due to its strong tropospheric warming such that the response of surface temperature changes to a strong tropospheric warming could be better observed. The simulation exhibits a linear, statistically significant EDW signal with warming ranging from $\sim 4.9K$ below 500m to almost 7K above 5500m and a regressed slope of 0.32 K/km; where this linear slope is used as a proxy to quantify EDW. The linearity and magnitude, both in global and regional analysis, is consistent with many previous studies, despite differences in experiment type and data used. Regional analysis further revealed that regional warming differences are primarily driven by the lowest bins, whereas at intermediate and high elevations regional ΔT_s profiles appear to converge. More specifically they seem to converge to the corresponding warming of the troposphere at those heights. Differently, the seasonal analysis revealed non-linear surface warming profiles, with variations possibly attributable to snow cover changes. However, comparison of these profiles to seasonal tropospheric warming suggested that, while snow changes and other factors may cause and explain some variability, most of the warming variability across seasons can be explained by seasonal variability in tropospheric warming. Overall, the comparison between binned surface and tropospheric warming across regions, elevations, and seasons reveals a remarkably tight coupling between the two. The linear regression in Figure 5 effectively averages over the many degrees of freedom in Equation 3, yet still shows that most points fall close to or slightly above the 1-to-1 line. This indicates that large-scale free-tropospheric warming provides a first-order control on surface warming at corresponding elevations, while surface energy-balance processes reflected in a positive mean offset ($\beta > 0$), mainly generate secondary deviations. Outliers, such as the systematically enhanced warming in the southern extratropics, reflect either genuinely local physical influences or the scarcity of grid cells in certain regions, and lie beyond the scope of this study. Taken together, these results suggest that EDW, as quantified

here, can be approximated to first order by the change in lapse rate of the lower troposphere, or equivalently by the slope of the regional tropospheric warming profile. The fitted values ($\alpha \approx 0.97$, $\beta \approx 0.57$ K) summarize this behavior but conceal its dependence on height, season, and region—dependencies that future work should resolve. Finally, it is important to note that this strong coupling may arise partly because of the unusually large magnitude of tropospheric warming in the P4K experiment. Such strong free-tropospheric warming may overwhelm many surface energy-balance processes, limiting them to producing modest deviations around the tropospheric profile. In a scenario with weaker tropospheric warming or a smaller reduction in lapse rate, these surface processes could exert a comparatively larger influence on local surface warming and thus on the pattern and magnitude of EDW. The result could not also not be verified or compared to observations or reanalysis data due to the lack of necessary observational data and the low magnitude of tropospheric warming in reanalysis products. Further future work could also focus on the use of higher resolution, perhaps reaching the 5km suggested by Pepin et al. (2015). With higher resolution higher elevation bins would include more data points and therefore be more representative of trends. Furthermore, more data points would allow for a better representation of peaks and valleys and thus the representation of small-scale variability such as cold air pooling and inversions which could decouple surface and tropospheric warming.

Statements and Declarations

Acknowledgments. P. M.'s and M. G.'s work was funded by the Max Planck Institute for Meteorology. The simulations were produced in the Cloud-Circulation Coupling in a Changing Climate (C5) project with computing resources awarded by The European High Performance Computing Joint Undertaking, grant EHPC-EXT-2022E01-041. A thank you to Lukas Kluft and Romain Fiévet for running the simulations and the German Climate Computing Center (DKRZ) for the computational resources and data storage.

Data Availability. The specific ICON version and boundary conditions information used to generate the simulation analyzed in this study are available at https://doi.org/10.17617/3.6XXCJS. However the simulation output dataset is too large to be made available. All figures were produced using custom Python scripts based on standard scientific libraries. The analysis scripts used to generate the figures are available from the authors upon reasonable request.

Competing Interests. The authors have no relevant financial or non-financial interests to disclose.

Author Contributions. All authors contributed to the study conception and design. Simulation data analysis was performed by Pietro Martuzzi. The first draft of the manuscript was written by Pietro Martuzzi and all authors commented on previous versions of the manuscript. All authors read and approved the final manuscript.

Appendix A Regional land grid cells counts

Table A1 shows the number of land model grid points at each elevation bin for each of the regions and latitude bands analyzed. As previously stated, global refers only to latitudes between 50°S and 50°N to avoid unwanted effects related to prescribed sea ice.

Table A1 Number of land grid cells in each elevation band for global, zonal, and mountain regions.

Elevation band (m)	Global	Tropics	Subtropics S	Subtropics N	Extratropics S	Extratropics N	Alps	Tibet	Rockies	Andes
0–500	90691	30153	12477	19670	5750	22641	273	1784	1118	763
500–1000	32076	9304	4592	8112	1339	8729	202	307	1262	301
1000–1500	18131	4547	3364	2335	718	7167	77	709	1187	264
1500–2000	6808	1219	424	1197	167	3801	55	423	1210	157
2000–2500	3487	506	152	726	58	2045	40	407	694	158
2500–3000	1609	273	137	202	37	960	4	435	179	150
3000–3500	1047	147	150	94	24	632	0	454	52	184
3500–4000	1203	135	337	103	24	604	0	615	5	405
4000–4500	1407	127	288	169	15	808	0	968	0	371
4500–5000	1525	43	111	217	2	1152	0	1367	0	144
5000–5500	825	0	3	118	0	704	0	822	0	3
5500–6000	64	0	0	11	0	53	0	64	0	0
6000–6500	3	0	0	2	0	1	0	3	0	0

References

Byrne, M.P., Boos, W.R., Hu, S.: Elevation-dependent warming: observations, models, and energetic mechanisms. Weather and Climate Dynamics **5**(2), 763–777 (2024) https://doi.org/10.5194/wcd-5-763-2024

Chimborazo, O., Minder, J.R., Vuille, M.: Observations and Simulated Mechanisms of Elevation-Dependent Warming over the Tropical Andes. Journal of Climate **35**(3), 1021–1044 (2022) https://doi.org/10.1175/JCLI-D-21-0379.1 . Chap. Journal of Climate

Colman, R., Soden, B.J.: Water vapor and lapse rate feedbacks in the climate system. Reviews of Modern Physics **93**(4), 045002 (2021) https://doi.org/10.1103/RevModPhys.93.045002

Ceppi, P., Scherrer, S.C., Fischer, A.M., Appenzeller, C.: Revisiting Swiss temperature trends 1959–2008. International Journal of Climatology **32**(2), 203–213 (2012) https://doi.org/10.1002/joc.2260

Duan, A., Wu, G.: Change of cloud amount and the climate warming on the Tibetan Plateau. Geophysical Research Letters **33** (2006) https://doi.org/10.1029/2006GL027946

Frierson, D.M.W.: Robust increases in midlatitude static stability in simulations of global warming. Geophysical Research Letters **33**(24) (2006) https://doi.org/10.1029/2006GL027504

Giorgetta, M.A., Brokopf, R., Crueger, T., Esch, M., Fiedler, S., Helmert, J., Hohenegger, C., Kornblueh, L., Köhler, M., Manzini, E., Mauritsen, T., Nam, C., Raddatz, T., Rast, S., Reinert, D., Sakradzija, M., Schmidt, H., Schneck, R., Schnur, R., Silvers, L., Wan, H., Zängl, G., Stevens, B.: ICON-A, the Atmosphere Component of the ICON Earth System Model: I. Model Description. Journal of Advances in Modeling Earth Systems **10**(7), 1613–1637 (2018) https://doi.org/10.1029/2017MS001242

Giorgi, F., Hurrell, J.W., Marinucci, M.R., Beniston, M.: Elevation Dependency of the Surface Climate Change Signal: A Model Study. Journal of Climate **10**(2), 288–296 (1997) https://doi.org/10.1175/1520-0442(1997)010⟨0288:EDOTSC⟩2.0.CO;2 . Chap. Journal of Climate

Hohenegger, C., Korn, P., Linardakis, L., Redler, R., Schnur, R., Adamidis, P., Bao, J., Bastin, S., Behravesh, M., Bergemann, M., Biercamp, J., Bockelmann, H., Brokopf, R., Brüggemann, N., Casaroli, L., Chegini, F., Datseris, G., Esch, M., George, G., Giorgetta, M., Gutjahr, O., Haak, H., Hanke, M., Ilyina, T., Jahns, T., Jungclaus, J., Kern, M., Klocke, D., Kluft, L., Kölling, T., Kornblueh, L., Kosukhin, S., Kroll, C., Lee, J., Mauritsen, T., Mehlmann, C., Mieslinger, T., Naumann, A.K., Paccini, L., Peinado, A., Praturi, D.S., Putrasahan, D., Rast, S.,

Riddick, T., Roeber, N., Schmidt, H., Schulzweida, U., Schütte, F., Segura, H., Shevchenko, R., Singh, V., Specht, M., Stephan, C.C., Storch, J.-S., Vogel, R., Wengel, C., Winkler, M., Ziemen, F., Marotzke, J., Stevens, B.: ICON-Sapphire: simulating the components of the Earth system and their interactions at kilometer and subkilometer scales. Geoscientific Model Development **16**(2), 779–811 (2023) https://doi.org/10.5194/gmd-16-779-2023

Held, I.M., Soden, B.J.: Robust Responses of the Hydrological Cycle to Global Warming. Journal of Climate **19**(21), 5686–5699 (2006) https://doi.org/10.1175/JCLI3990.1 . Chap. Journal of Climate

IPCC: High mountain areas. In: The Ocean and Cryosphere in a Changing Climate, pp. 131–202. Cambridge University Press, Cambridge (2022). https://doi.org/10.1017/9781009157964.004

IPCC: Climate change 2023: Synthesis report. contribution of working groups i, ii and iii to the sixth assessment report of the intergovernmental panel on climate change. Technical report, Intergovernmental Panel on Climate Change, Geneva, Switzerland (2023). https://doi.org/10.59327/IPCC/AR6-9789291691647 . https://www.ipcc.ch/report/ar6/syr/

Kotlarski, S., Bosshard, T., Lüthi, D., Pall, P., Schär, C.: Elevation gradients of European climate change in the regional climate model COSMO-CLM. Climatic Change **112**(2), 189–215 (2012) https://doi.org/10.1007/s10584-011-0195-5

Liu, X., Chen, B.: Climatic warming in the Tibetan Plateau during recent decades. International Journal of Climatology **20**(14), 1729–1742 (2000) https://doi.org/10.1002/1097-0088(20001130)20:14⟨1729::AID-JOC556⟩3.0.CO;2-Y

Liu, X., Cheng, Z., Yan, L., Yin, Z.-Y.: Elevation dependency of recent and future minimum surface air temperature trends in the Tibetan Plateau and its surroundings. Global and Planetary Change **68**(3), 164–174 (2009) https://doi.org/10.1016/j.gloplacha.2009.03.017

La Sorte, F.A., Jetz, W.: Projected range contractions of montane biodiversity under global warming. Proceedings of the Royal Society B: Biological Sciences **277**(1699), 3401–3410 (2010) https://doi.org/10.1098/rspb.2010.0612

Merlis, T.M., Guendelman, I., Cheng, K.-Y., Harris, L., Chen, Y.-T., Bretherton, C.S., Bolot, M., Zhou, L., Kaltenbaugh, A., Clark, S.K., Fueglistaler, S.: The Vertical Structure of Tropical Temperature Change in Global Storm-Resolving Model Simulations of Climate Change. Geophysical Research Letters **51**(23), 2024–111549 (2024) https://doi.org/10.1029/2024GL111549

Minder, J.R., Letcher, T.W., Liu, C.: The Character and Causes of Elevation-Dependent Warming in High-Resolution Simulations of Rocky Mountain Climate Change. Journal of Climate **31**(6), 2093–2113 (2018) https://doi.org/10.1175/

JCLI-D-17-0321.1 . Chap. Journal of Climate

Ohmura, A.: Enhanced temperature variability in high-altitude climate change. Theoretical and Applied Climatology **110**(4), 499–508 (2012) https://doi.org/10.1007/s00704-012-0687-x

Pepin, N.C., Arnone, E., Gobiet, A., Haslinger, K., Kotlarski, S., Notarnicola, C., Palazzi, E., Seibert, P., Serafin, S., Schöner, W., Terzago, S., Thornton, J.M., Vuille, M., Adler, C.: Climate Changes and Their Elevational Patterns in the Mountains of the World. Reviews of Geophysics **60**(1), 2020–000730 (2022) https://doi.org/10.1029/2020RG000730

Pepin, N., Bradley, R.S., Diaz, H.F., Baraer, M., Caceres, E.B., Forsythe, N., Fowler, H., Greenwood, G., Hashmi, M.Z., Liu, X.D., Miller, J.R., Ning, L., Ohmura, A., Palazzi, E., Rangwala, I., Schöner, W., Severskiy, I., Shahgedanova, M., Wang, M.B., Williamson, S.N., Yang, D.Q., Mountain Research Initiative EDW Working Group: Elevation-dependent warming in mountain regions of the world. Nature Climate Change **5**(5), 424–430 (2015) https://doi.org/10.1038/nclimate2563

Palazzi, E., Filippi, L., Hardenberg, J.: Insights into elevation-dependent warming in the Tibetan Plateau-Himalayas from CMIP5 model simulations. Climate Dynamics **48**(11), 3991–4008 (2017) https://doi.org/10.1007/s00382-016-3316-z

Pepin, N.C., Lundquist, J.D.: Temperature trends at high elevations: Patterns across the globe. Geophysical Research Letters **35**(14) (2008) https://doi.org/10.1029/2008GL034026

Palazzi, E., Mortarini, L., Terzago, S., Von Hardenberg, J.: Elevation-dependent warming in global climate model simulations at high spatial resolution. Climate Dynamics **52**(5-6), 2685–2702 (2019) https://doi.org/10.1007/s00382-018-4287-z

Qixiang, W., Wang, M., Fan, X.: Seasonal patterns of warming amplification of high-elevation stations across the globe. International Journal of Climatology **38**(8), 3466–3473 (2018) https://doi.org/10.1002/joc.5509

Rottler, E., Kormann, C., Francke, T., Bronstert, A.: Elevation-dependent warming in the Swiss Alps 1981–2017: Features, forcings and feedbacks. International Journal of Climatology **39**(5), 2556–2568 (2019) https://doi.org/10.1002/joc.5970

Rupp, D.E., Li, S., Mote, P.W., Shell, K.M., Massey, N., Sparrow, S.N., Wallom, D.C.H., Allen, M.R.: Seasonal spatial patterns of projected anthropogenic warming in complex terrain: a modeling study of the western US. Climate Dynamics **48**(7), 2191–2213 (2017) https://doi.org/10.1007/s00382-016-3200-x

Rangwala, I., Miller, J.R., Russell, G.L., Xu, M.: Using a global climate model to evaluate the influences of water vapor, snow cover and atmospheric aerosol on warming in the Tibetan Plateau during the twenty-first century. Climate Dynamics **34**(6),

859–872 (2010) https://doi.org/10.1007/s00382-009-0564-1

Rangwala, I., Miller, J.R., Xu, M.: Warming in the Tibetan Plateau: Possible influences of the changes in surface water vapor. Geophysical Research Letters **36**(6) (2009) https://doi.org/10.1029/2009GL037245

Rangwala, I., Sinsky, E., Miller, J.R.: Amplified warming projections for high altitude regions of the northern hemisphere mid-latitudes from CMIP5 models. Environmental Research Letters **8**(2), 024040 (2013) https://doi.org/10.1088/1748-9326/8/2/024040

Rangwala, I., Sinsky, E., Miller, J.R.: Variability in projected elevation dependent warming in boreal midlatitude winter in CMIP5 climate models and its potential drivers. Climate Dynamics **46**(7), 2115–2122 (2016) https://doi.org/10.1007/s00382-015-2692-0

Tudoroiu, M., Eccel, E., Gioli, B., Gianelle, D., Schume, H., Genesio, L., Miglietta, F.: Negative elevation-dependent warming trend in the Eastern Alps. Environmental Research Letters **11**(4), 044021 (2016) https://doi.org/10.1088/1748-9326/11/4/044021

Taylor, K.E., Williamson, D., Zwiers, F.: PCMDI Report - Number 60 - The sea surface temperature and sea-ice concentration boundary conditions for AMIP II simulations. Technical report, Zenodo (September 2000). https://doi.org/10.5281/zenodo.13835219 . https://zenodo.org/records/13835219

Wang, Q., Fan, X., Wang, M.: Recent warming amplification over high elevation regions across the globe. Climate Dynamics **43**(1), 87–101 (2014) https://doi.org/10.1007/s00382-013-1889-3

Wang, Q., Fan, X., Wang, M.: Evidence of high-elevation amplification versus Arctic amplification. Scientific Reports **6**(1), 19219 (2016) https://doi.org/10.1038/srep19219

Whiteman, C.D.: Mountain Meteorology: Fundamentals and Applications. Oxford University Press, ??? (2000). https://doi.org/10.1093/oso/9780195132717.001.0001 . https://doi.org/10.1093/oso/9780195132717.001.0001

Yan, L., Liu, Z., Chen, G., Kutzbach, J.E., Liu, X.: Mechanisms of elevation-dependent warming over the Tibetan plateau in quadrupled CO2 experiments. Climatic Change **135**(3), 509–519 (2016) https://doi.org/10.1007/s10584-016-1599-z